IEEE Access
Multidisciplinary ⋮ Rapid Review ⋮ Open Access Journal

Received 6 January 2023, accepted 21 January 2023, date of publication 30 January 2023, date of current version 3 February 2023.

*Digital Object Identifier 10.1109/ACCESS.2023.3240896*

RESEARCH ARTICLE

# A 3.6 GHz Polar Reflection-Type Vector Modulator Phase Shifter With Amplitude Control Capability

**RAUL ARRUELA[1,2], (Graduate Student Member, IEEE), TIAGO VARUM[1], (Member, IEEE), AND JOÃO NUNO MATOS[1,2], (Member, IEEE)**
Instituto de Telecomunicações, Universitário de Santiago, 3810-193 Aveiro, Portugal
Departamento de Eletrónica, Telecomunicações e Informática, Universidade de Aveiro, 3810-193 Aveiro, Portugal

Corresponding author: Tiago Varum (tiago.varum@ua.pt)

This work was funded by the Fundação para a Ciência e Tecnologia (FCT)/Ministério da Ciência, Tecnologia e Ensino Superior (MCTES) through national funds and, when applicable, co-funded EU funds under the project UIDB/50008/2020-UIDP/50008/2020. The work was also supported by the FCT through Fundo Social Europeu (FSE) and by the Programa Operacional Regional do Centro (CENTRO 2020), under the PhD grant 2021.08900.BD.

**ABSTRACT** This paper presents a new passive vector modulator phase shifter (VMPS) based on a polar architecture suitable for use in advanced beamforming feeding networks. The cascaded structure of a reflection-type bi-phase variable attenuator (RTBVA) and a reflection-type phase shifter (RTPS) allows great flexibility regarding phase and amplitude control, and reduces amplitude errors in phase shifting. A printed circuit operating at a central frequency of 3.6 GHz with 5-bit phase resolution was designed and implemented to validate the proposed concept. The measured results showed a 360° phase shift range, an average insertion loss of 2.4 dB at 3.6 GHz, a root-mean-square phase, and a gain error of 1.3° and 0.06 dB, respectively. This VMPS also allows an amplitude control range of ∼25 dB and an operational bandwidth of 0.7 GHz (19.4%).

**INDEX TERMS** Vector modulator, polar modulation, phase shifter, attenuator, reflection-type, phased array, beamforming.

## I. INTRODUCTION

Wireless communications are being increasingly explored in response to the growing daily demand for a smarter and more connected world. In this sense, communications with high data transmission rates, low latency, and support for many users and devices are simultaneously required. In response to this technological progress, phased-array antennas are one of the key technologies adopted to satisfy such requirements [1], [2], [3], [4].

Phased arrays are frequently composed of equally spaced radiating elements, where the feeding of each antenna element is controlled independently, both in terms of amplitude and phase. By manipulating the feeding of each element, it is possible to modify and steer the radiation pattern of the entire array. This technique of adjusting the feeding of an antenna array is known as beamforming. In addition to other advantages, beamforming enables spatial filtering, reducing interferences in communications, whether intentional or unintentional. Beamforming can be implemented in the analog (RF, LO, or IF) or digital domains (BB). Digital beamforming would be more easily applied; however, given the need for an ADC/DAC and a complete RF chain for each antenna element, as the number of radiating elements increases (e.g., large-scale arrays with thousands of elements), it would quickly become unfeasible. Currently, for large-scale antenna arrays, both from a technical point of view (an extremely high amount of data to process and the consequent energy consumption) and in terms of cost, digital beamforming is almost impracticable. Analog beamforming systems require additional devices, the most common are phase shifters or vector modulators (VM), to control the feeding of each element, changing the amplitude and/or phase.

The associate editor coordinating the review of this manuscript and approving it for publication was Ludovico Minati.

Analog phase shifters can be passive or active. Nevertheless, the passive ones provide more linearity and zero (or negligible) power consumption. The most common phase-shifter structures are the Switched-Delay Lines [5] (which are inherently digital and do not allow continuous phase variation), the Loaded-Line [6], the RTPS [7], [8], [9], [10] and the VM [11]. VMs can allow a 360° phase variation range and amplitude control. Typically, a VM consists of the sum of two signal components, in-phase and quadrature (I and Q) [12]. Some variants of the IQ-VM have been presented in the literature for beamforming and applications in direct modulation transmitters, given the attractive benefit it can bring about in reducing its complexity and cost. In [13], two active IQ-VMs using 28 nm FDSOI CMOS technology designed to operate at central frequencies of 87.4 GHz and 89.2 GHz were presented. They used a modified coupled line quadrature coupler to split the input signal into two orthogonal signals, I and Q, and then used a VGA to control the amplitude of both signals before combining them in the output signal. The 87.4 GHz active IQ-VM has an average gain of 2.3 dB, and the 89.2 GHz has 0.83 dB, each consuming 21.6 mW.

In [14], a 24 GHz reflection-type IQ-VM (IQ-RTVM) fabricated in a PCB and applied to a phased array was presented. It consists of a Wilkinson power divider that splits the input signal into two branches, I and Q, followed by an RTBVA constructed with PIN diodes that control the amplitude of both signals before they are added with a Wilkinson power combiner at the output. In [15], were presented two balanced IQ-RTVMs designed using MMIC technology operating at 38 GHz and 60 GHz, with a bandwidth of 20 GHz and an average insertion loss of 5 dB, for use in direct multilevel carrier modulation. In this case, cold-pHEMT (0 Vdc is applied at the drain) transistors are used instead of PIN diodes to reduce the biasing DC power consumption. In [16], a more compact balanced IQ-RTVM was presented, using four hybrid couplers designed on a 0.25 $\mu$m SiGe BiCMOS technology to operate between 18.3-22.4 GHz. It has 9.6 dB of insertion loss at the central frequency and no DC power consumption.

IQ-VMs have the disadvantage of an inherent power loss of 3 dB resulting from combining signals I and Q at the output. Moreover, it will be extended to 6 dB if it is considered the region where the VM manages to perform the entire 360° phase-shifting range with constant amplitude, which is necessary for beamforming.

Although the IQ-VM is the architecture most found in the literature, an alternative topology consists of a phase shifter followed by a variable gain amplifier (VGA), also known as Polar-VM. A Polar-VM is shown in [17], where the phase shifter is composed of two circulators that allow a range of phase variation slightly over 180° and a differential VGA that provides control of the amplitude and the phase inversion needed to reach 360°. In [18], was presented a 60 GHz active Polar VM, constructed under an IQ architecture and used a look-up-table (LUT) based calibration process to generate a polar constellation.

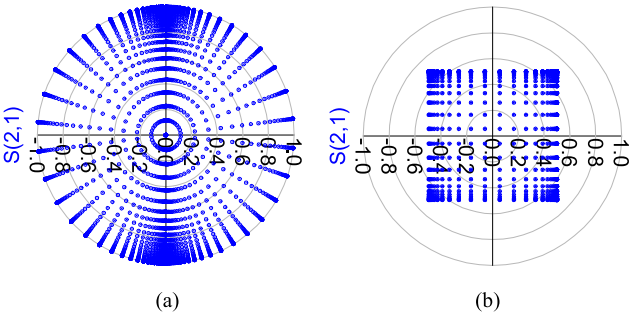


**FIGURE 1.** Ideal $S_{21}$ constellation: (a) Polar reflection-type vector modulator (b) IQ reflection-type vector modulator.

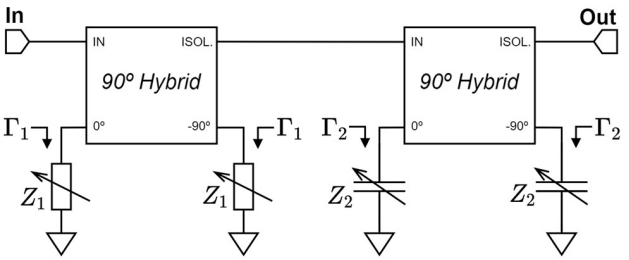


**FIGURE 2.** Block diagram of the proposed Polar-reflection type vector modulator.

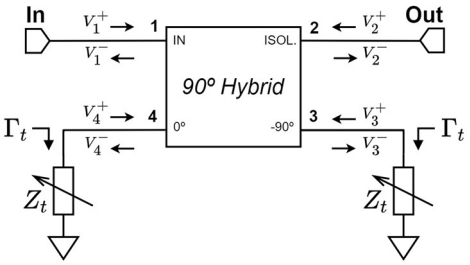


**FIGURE 3.** Block diagram of a reflection type bi-phase variable attenuator.

This paper proposes a new passive vector modulator phase shifter. In contrast to IQ-VMPS, this Polar Reflection-Type VMPS (Polar-RTVMPS) does not suffer from inherent losses such as the 3 dB (or 6 dB) mentioned above. As a cascade structure, it does not require power dividers/combiners, making it simpler and more compact, thereby reducing the overall losses in practical implementations. Fig. 1 illustrates the differences between the (ideal) constellations of the Polar-RTVM and IQ-RTVM.

The remainder of this paper is organized as follows. Section II presents the proposed Polar-RTVMPS and explains each of its building blocks, followed by the prototype design. Section III presents the simulation results obtained from Polar-RTVMPS. In Section IV, a characterization of the designed prototype is presented. Finally, the main conclusions are summarized in Section V.

## II. PROPOSED VECTOR MODULATOR PHASE SHIFTER

### A. POLAR-RTVMPS

The proposed VMPS uses two cascaded blocks, an RTBVA, followed by an RTPS, as shown in Fig. 2. The first unit works as a variable attenuator and phase inverter. The second block has the function of a phase shifter.

The common RTPS has limitations regarding the range of phase shifting, as will be demonstrated later. The capability of phase inversion in the variable attenuator is crucial to solving this problem, allowing, in a simple way, obtaining a 360° phase shifting range while having amplitude control capability.

The S-parameter matrix of the Polar-RTVMPS can be obtained from the RTBVA (sub-section B) and RTPS (sub-section C) S-parameters, converting each one into its corresponding ABCD matrix, multiplying them, and then convert it back to S-parameters, resulting in the following expression

$$[S] = \begin{bmatrix} 0 & -\Gamma_1\Gamma_2 \\ -\Gamma_1\Gamma_2 & 0 \end{bmatrix} \tag{1}$$

where $\Gamma_1$ and $\Gamma_2$ are the reflection coefficients of the RTVBA and RTPS loads, respectively. The magnitude and phase of $S_{21}$ are as follows,

$$|S_{21}| = |\Gamma_1| \tag{2}$$

$$\angle S_{21} = sign\,(\Gamma_1)\,\Phi_{\Gamma_2} \tag{3}$$

where $\Phi_{\Gamma_2}$ is the phase of the RTPS load's reflection coefficient.

### B. RTBVA

An RTBVA comprises a 90° hybrid coupler terminated with two (equal) variable resistive loads, as shown in Fig.3. The analysis was performed using the matrix of S-parameters of an ideal 90° hybrid coupler. The input of the attenuator is located at port 1 (input), the output is located at port 2 (ISOL), and the resistive loads ($Z_t$) are placed in transmission ports 3(−90°) and 4 (0°).

When the value of the resistances is equal to the characteristic impedance ($Z_0$) of the hybrid coupler, ports 3 and 4 are matched, and the resistances absorb all the energy applied in port 1. Under these circumstances, no energy is transferred to port 2, resulting in the particular case of maximum attenuation. The other two special situations occur when the resistances are assumed to be 0 Ω and a high value (theoretically infinite). In these cases, the attenuation has the minimum value given that all the energy applied at the RTBVA input is reflected in transmission ports 3 and 4 and transferred to the output.

In addition to these conditions, two regions should be considered. The first is when the value of the resistances is between 0 and $Z_0$, where the attenuation varies from 0 to infinity. In the second region, when this value is between $Z_0$ and infinity, the attenuation varies from infinity to 0, respectively. Another important aspect is that the sign of the reflection coefficient in the resistors changes when it crosses the $Z_0$, allowing a phase inversion in the RTVBA, as shown in Equation (4).

$$\Gamma_t = \frac{Z_t - Z_0}{Z_t + Z_0} \tag{4}$$

The next Equation allows us to obtain the S-parameters of the RTBVA, which was obtained by analyzing Fig. 3 and from the S-parameter matrix of an ideal 90° hybrid coupler, which can be expressed as

$$\begin{bmatrix} V_1^- \\ V_2^- \\ V_3^- \\ V_4^- \end{bmatrix} = -\frac{1}{\sqrt{2}} \begin{bmatrix} 0 & 0 & 1 & j \\ 0 & 0 & j & 1 \\ 1 & j & 0 & 0 \\ j & 1 & 0 & 0 \end{bmatrix} \begin{bmatrix} V_1^+ \\ V_2^+ \\ V_3^+ \\ V_4^+ \end{bmatrix}. \tag{5}$$

Assuming that the loads are equal, i.e.,

$$\Gamma_t = \frac{V_3^+}{V_3^-} = \frac{V_4^+}{V_4^-} \tag{6}$$

it gives

$$S_{21} = j\Gamma_t. \tag{7}$$

And so, the attenuation of the RTBVA is

$$|S_{21}| = |\Gamma_t| \tag{8}$$

and its phase shifting

$$\angle S_{21} = \frac{\pi}{2} sign\,(\Gamma_t)\,. \tag{9}$$

Knowing that $V_3^+ = -jV_4^+$, we get

$$S_{11} = 0 \tag{10}$$

and from the symmetry of the circuit

$$S_{22} = 0. \tag{11}$$

### C. RTPS

In the case of the RTPS, the principle of operation is the same as that explained for the RTBVA. However, instead of resistive terminations, there are reactive terminations. These loads naturally present a unitary reflection coefficient; therefore, all the energy applied in port 1 (input) is transferred to port 2 (output). Thus, the insertion loss of the phase shifter is (theoretically) always zero.

The RTPS typically uses variable capacitors (varactors) for reactive terminations. Ideally, a capacitive reactance assuming values from 0 to infinity, would create a reflection coefficient ranging from 0° to −180°, respectively. In practice, this range is reduced owing to the component limitations. However, there are techniques to overcome this problem at the expense of an increase in the complexity of the circuit, which will certainly be reflected in more losses.

The S parameters of the RTPS were obtained using Equation (5), which led to similar results.

$$S_{21} = j\Gamma_t \tag{12}$$

$$|S_{21}| = |\Gamma_t| \tag{13}$$

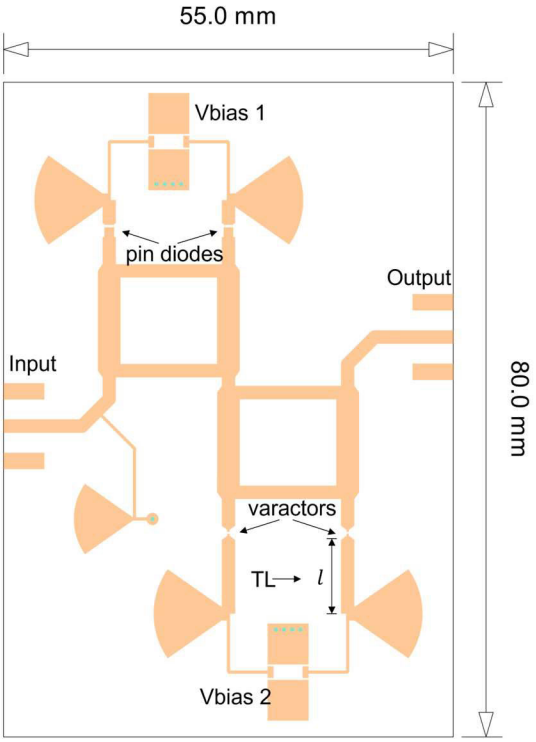


**FIGURE 4.** Layout of the designed Polar-RTVM.

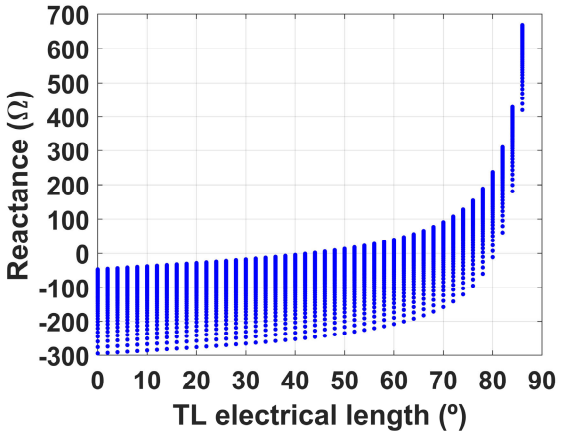


**FIGURE 5.** The reactance of the TL and varactor in series.

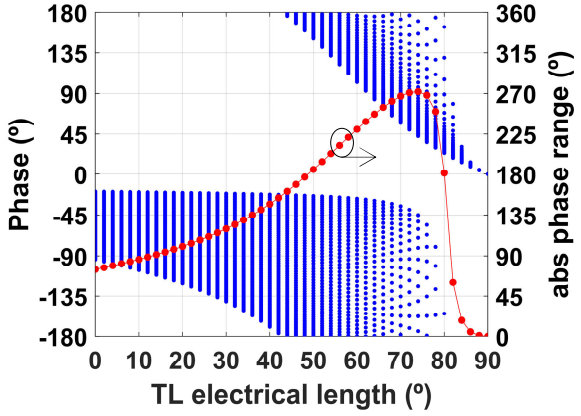


**FIGURE 6.** Phase (blue) and absolute phase range (i.e., the interval size) of the reflection coefficient of the TL and varactor in series for many values of TL electrical length.

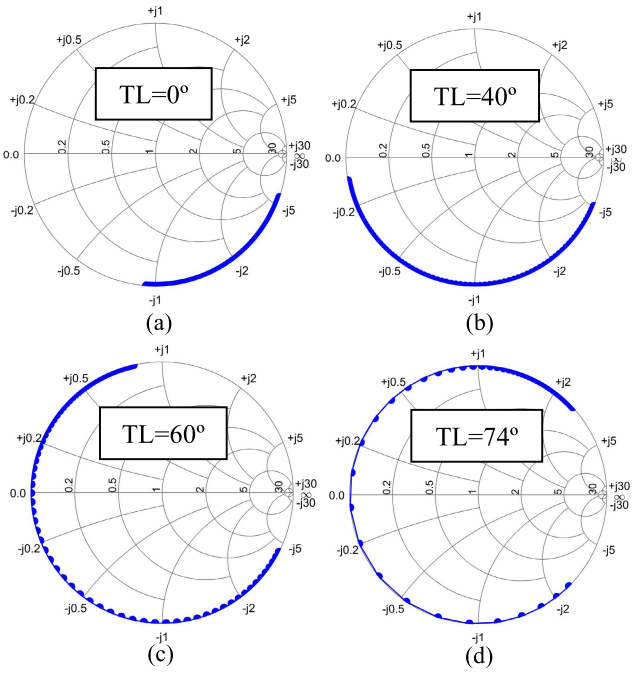


**FIGURE 7.** Impedance of the TL and varactor in series, for various electrical lengths (a) TL=0°, (b) TL=40°, (c) TL=60° and (d) TL=74°.

In this case, the magnitude of $S_{21}$ is (theoretically) unitary, and its phase

$$\angle S_{21} = \frac{\pi}{2} + \Phi_{\Gamma_t} \tag{14}$$

where $\Phi_{\Gamma_t}$ is the phase of the load reflection coefficient. The $S_{11}$ and $S_{22}$ are also equal to zero.

### D. POLAR-RTVMPS DESIGN

To prove the concept presented, a Polar-RTVM was designed to operate at 3.6 GHz, printed on a RO4350B substrate with dielectric constant $\varepsilon_r = 3.66$ (thickness $h = 0.76$ mm), using transmission lines with microstrip technology and with characteristic impedance $Z_0 = 50\ \Omega$. The designed circuit is shown in Fig. 4. It consists of two 90° hybrid couplers, two PIN diodes, and two varactor diodes. A thin transmission line with $Z_0 = 100\ \Omega$ can be observed next to the input port, followed by a radial stub and a via, allowing a DC ground for biasing the four diodes.

Because the varactors do not allow a reflection coefficient with a 180° phase range (only an ideal varactor would do so), an inductance implemented by a short-circuit terminated transmission line (TL) was placed in series with each varactor to extend the range to 180° or higher.

Calculations were performed using Equation (15) for different lengths to obtain the necessary TL length.

This Equation represents the impedance obtained with the series of a short-circuit terminated TL and a capacitor,

$$Z = j\left[Z_0 \tan(\beta l) - \frac{1}{\omega C}\right] \tag{15}$$

where $l$ is the TL length and C is the capacitance.

Fig.5 shows the results obtained for a TL with an electrical length ranging from 0° to 90° in steps of 2° and a capacitance ranging from 150 fF to 950 fF in steps of 10 fF, frequency of 3.6 GHz, and $Z_0 = 50\ \Omega$. As shown in Fig. 5, for each TL length, the reactance range is the same, and the only difference is the shift in the average value. However, the same does not occur in the phase range of the reflection coefficient. In fact, it varies considerably, as shown in Fig. 6. It shows the phase range (red) and has a maximum at TL=74°. Moreover, in Figs. 7 (a), (b), (c), and (d) is shown Smith charts where it is easier to observe that for the four cases, the reactance range is always the same, and only the range of the reflection coefficient's phase varies. The latter has its maximum when the center of its range coincides with Smith chart's short circuit. In the case of TL=0°, the reflection coefficient phase range is the smallest and corresponds only to the varactor itself. In this case, the range is insufficient; the same happens for TL=40°. On the other hand, for TL=60°, the range is clearly above 180°, making this TL electrical length more than enough for the Polar-RTVM phase shifting. It is also shown that a higher phase range can be obtained with TL=74°.

Further, with the help of the inverter block, a 360° phase range is achieved. The length of the transmission line between the PIN diode and the radial stub was also optimized to compensate for its parasitic elements. The chosen PIN diodes are the Microchip's MMP4401-GM2, which serve as variable resistance elements (approx. between 0.8 Ω and 5k Ω) and are forward biased through Vbias1 (approx. between 0.4 V and 0.9 V). The selected varactor diodes are the MAVR-000120-14110P from MACOM, which work as variable capacitance elements (approx. between 0.15 pF and 0.9 pF) and are reverse biased through Vbias2 (approx. between 1 V and 12 V).

## III. SIMULATION RESULTS

Simulations of the circuit in Fig. 4 were performed using the Advanced Design System software (ADS), considering the diode's high-frequency models (including parasitics). The resistance of the PIN diodes was swept from 0.8 Ω to 5k Ω, and the capacitance of the varactors was changed from 0.15 pF to 0.9 pF. It was simulated between 3.2 GHz and 3.9 GHz, with steps of 50 MHz, to evaluate the circuit behaviour across the frequencies. Fig. 8 shows the constellation of points (blue) representing the parameter $S_{21}$ at 3.6 GHz for 4872 resistance and capacitance value combinations. Additionally, it shows 32 selected points (red) chosen to achieve an 11.25° resolution phase shift with 360° of a shifting range, aiming simultaneously for minimum insertion loss and amplitude/phase errors. This procedure was performed over the entire frequency range, resulting in a different LUT

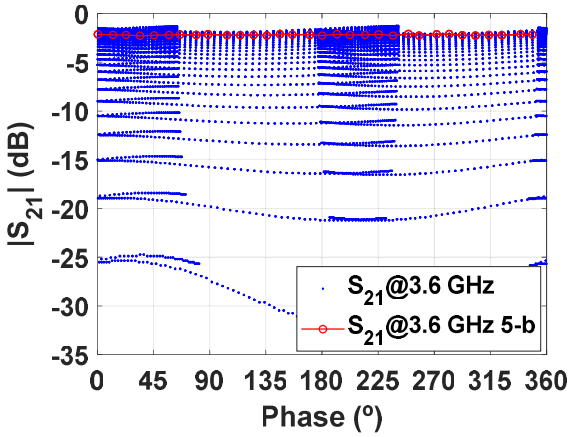


**FIGURE 8.** Gain versus phase @3.6 GHz for all simulated points (blue) and the 5-bit selected points (red).

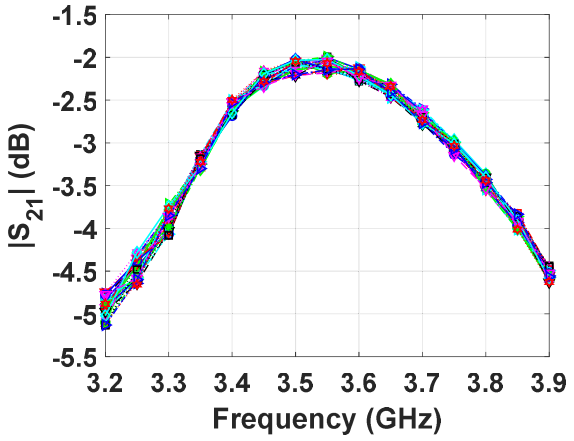


**FIGURE 9.** Simulated gain for the 32 selected states chosen for each frequency.

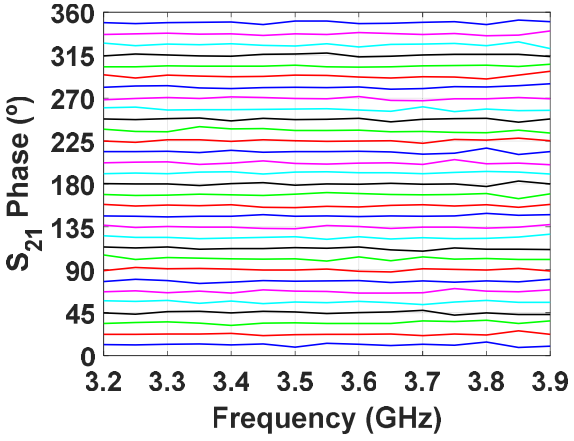


**FIGURE 10.** Simulated relative phase shift for the 32 selected states chosen for each frequency.

for each frequency. Fig. 9 shows the gain of each of the 32 selected points across the frequencies. It presents a gain variation of $< 0.5$ dB at each frequency and a maximum gain of $-2$ dB at 3.55 GHz. It also shows that the bandwidth

of the designed Polar-RTVM phase shifter is approximately 700 MHz, considering the range where the gain drops by 3 dB. Fig. 10 shows the relative phase shifts for all 32 states at each frequency. The 32 horizontal lines are not entirely flat, showing some phase errors, that is, deviations from the targeted phase shift.

The root-mean-square (RMS) phase and gain errors were calculated from Fig. 10 and Fig. 9, respectively, using Eqs. 16 and 17.

$$\theta_{RMS,\text{error}} = \sqrt{\frac{1}{N-1} \times \sum_{i=2}^{N} \left|\theta_i - \theta_{i,ideal}\right|^2} \quad (16)$$

$$A_{RMS,\text{error}} = \sqrt{\frac{1}{N} \times \sum_{i=1}^{N} \left|A_i - A_{avg}\right|^2} \quad (17)$$

The results are shown in Fig. 11. The RMS phase error is <2.3°, and the RMS gain error is <0.13 dB in the entire bandwidth. Fig. 12 shows the input/output reflection coefficients of the designed Polar-RTVM, $|S_{11}|$, and $|S_{22}|$ for the 32 selected states chosen for each frequency. It can be observed that both parameters are below −10 dB from 3.5 to 3.9 GHz. It is worth mentioning that although it seems like above 3.9 GHz the Polar-RTVM could present good results regarding return losses, the simulation revealed that the 360° of the required phase shift range was not achieved, and also the gain dropped considerably.

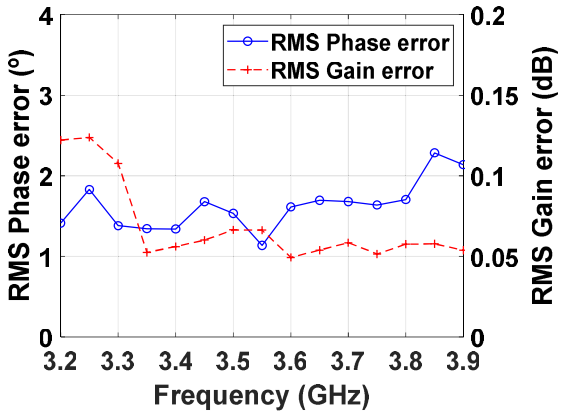


**FIGURE 11.** Simulated RMS phase and gain error.

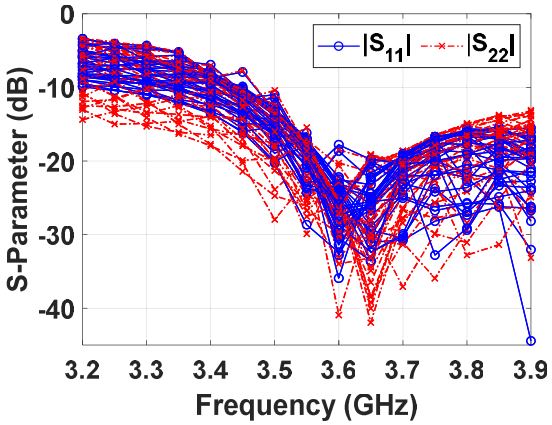


**FIGURE 12.** Simulated $|S_{11}|$ and $|S_{22}|$ for the 32 selected states chosen for each frequency.

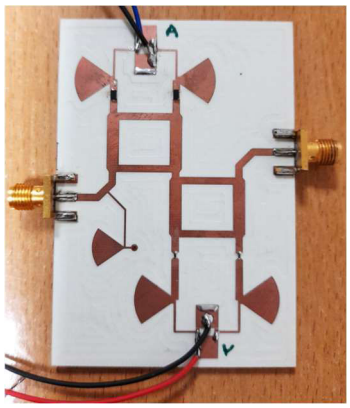


**FIGURE 13.** Photograph of the Polar-RTVM.

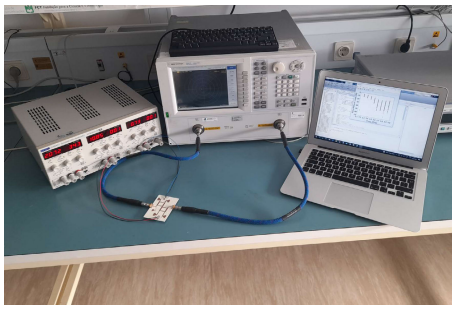

**FIGURE 14.** Photograph of the measurement setup.

## IV. MEASUREMENT RESULTS

Photographs of the fabricated prototype and the measurement setup are shown in Figs. 13 and 14, respectively. The measurement setup comprised a TTi PL303QMT-P programmable power supply, an Agilent PNA E8361C vector network analyzer and a PC. The S-Parameters were measured for a frequency range between 3.2 GHz and 3.9 GHz with a resolution of 50 MHz and 10201 combinations of bias voltages of the PIN diodes and varactors. The PIN diodes were forward biased through Vbias1 between 0 V and 0.85 V in 8.5 mV steps. The varactor diodes were reverse biased through Vbias2 between 0 V and 12 V in 120 mV steps. Fig. 15 shows all points (blue) that represent the parameter $S_{21}$ at 3.6 GHz for the 10201 combinations of bias voltages. It shows 32 selected points (red) chosen to achieve an 11.25° resolution phase shifter with 360° of phase shift range, aiming for minimum insertion loss and amplitude/phase errors. This procedure was performed for the entire bandwidth, resulting in a different LUT for each frequency. Fig. 16 shows the gain of each 32 selected points at each frequency,

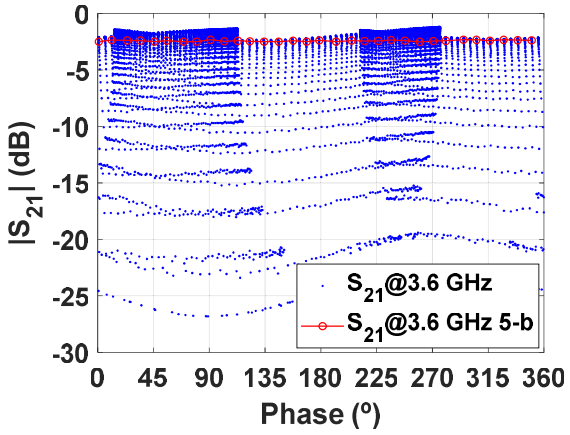


**FIGURE 15.** Gain versus phase @3.6 GHz for all measured points (blue) and the 5-bit selected points (red).

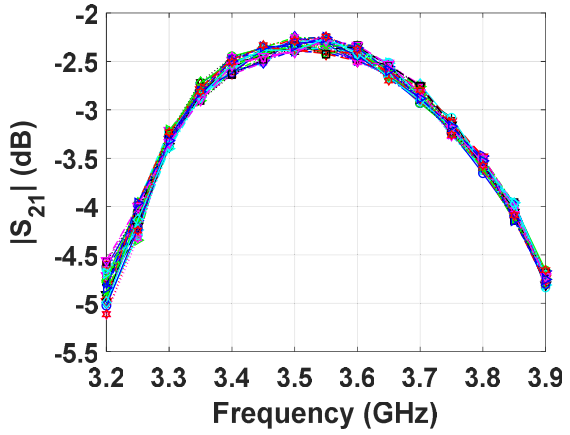


**FIGURE 16.** Measured gain for the 32 selected states chosen for each frequency.

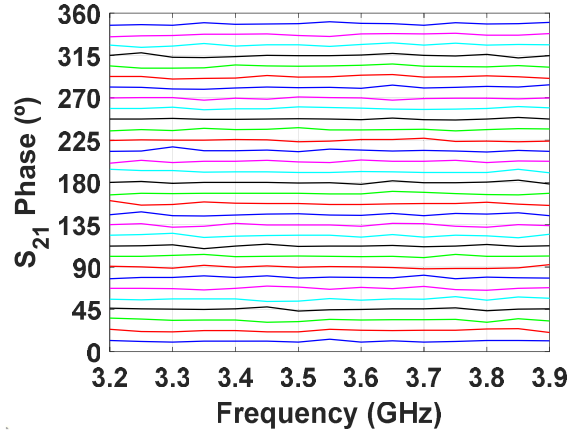


**FIGURE 17.** Measured relative phase shift for the 32 selected states chosen for each frequency.

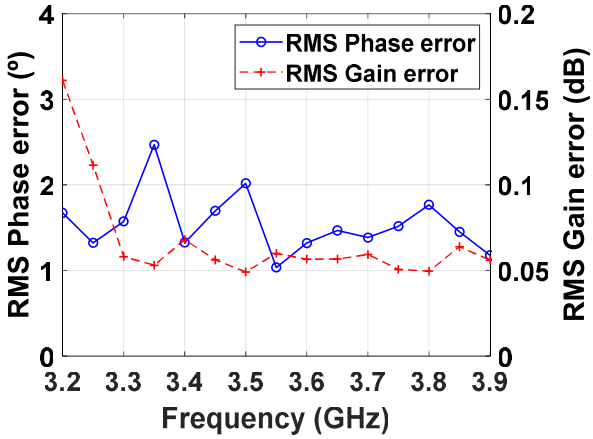


**FIGURE 18.** Measured RMS phase and gain error.

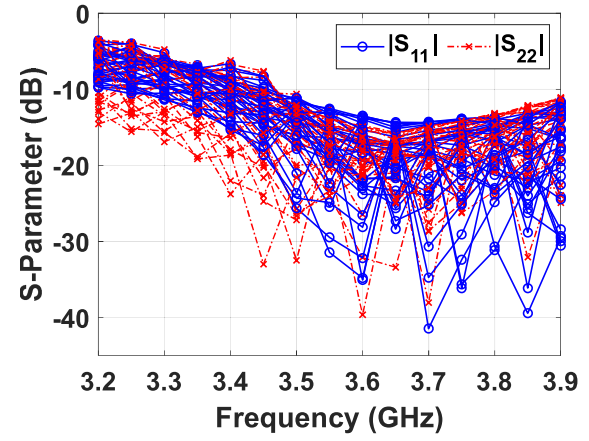


**FIGURE 19.** Measured $|S_{11}|$ and $|S_{22}|$ for the 32 selected states chosen for each frequency.

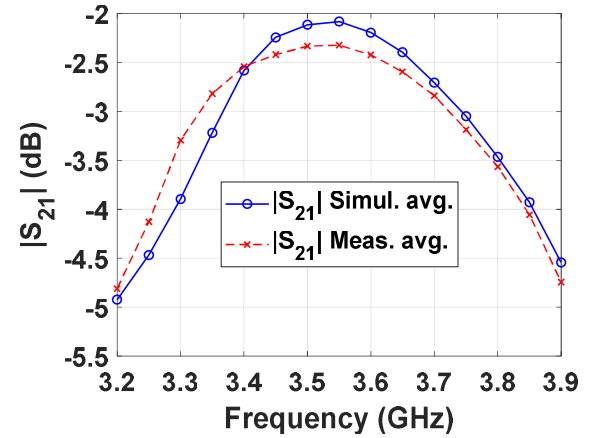


**FIGURE 20.** Comparison of the average gain simulated and measured.

demonstrating a gain variation of $< 0.5$ dB and a maximum gain of $-2.2$ dB at 3.55 GHz. It also shows that the 3-dB bandwidth is approximately 700 MHz. Fig. 17 presents the relative phase shifts for all 32 states across the frequencies. The RMS phase and gain errors were calculated from Figs. 17 and 16, respectively, using Equations 16 and 17, and the results are displayed in Fig. 18. The RMS phase error is always below 2.5°, and the RMS gain error is considerably small, and below 0.13 dB in the entire bandwidth. Regarding the input/output measured reflection coefficients, which are shown in Fig. 19 for all the 32 states, it can be observed that both $|S_{11}|$ and $|S_{22}|$ are below $-10$ dB, from 3.5 to 3.9 GHz.

**TABLE 1. Performance comparison with previous passive phase shifters.**

| Ref. | Technique | Freq. (GHz) | Phase Range (deg.) | Phase Resol. (bits) | Insertion Loss (dB) | RMS Phase Error (deg.) | RMS Gain Error (dB) | Amplitude Control Capability | Process | Circuit Size |
|---|---|---|---|---|---|---|---|---|---|---|
| This work | Polar-RTVMPS | 3.6 | 360 | 5 | 2.4 | 1.3 | 0.06 | Yes | PCB | 1.12 $\lambda_g$ × 1.63 $\lambda_g$ |
| [19] | VSPS | 0.75 ~ 0.95 | 360 | N/A | 5.27 ~ 6.62 | < 8.45 | < 2.58 | Yes | PCB | N/A |
| [20] | RTPS | 3.5 | 132.7 | N/A | 8.87 | N/A | N/A | Yes | 180 nm CMOS | 1.25 mm$^2$ |
| [9] | RTPS | 2 | 407 | N/A | 4.4 ± 0.2 | N/A | N/A | No | PCB | 0.32 $\lambda_g$ × 0.59 $\lambda_g$ |
| [21] | RTPS | 2 | 385 | N/A | 0.98 ± 0.58 | N/A | N/A | No | PCB | 0.27 $\lambda_g$ × 0.39 $\lambda_g$ |
| [22] | DA-RTPS | 29 | 360 | 5 | 6.8 ± 0.1 | 0.3 | N/A | No | 45 nm SOI | 0.065 mm$^2$ |
| [23] | RTTLPS | 28 | 180 | 5 | 17 ± 0.4 | 3 | N/A | Yes | 65 nm CMOS | 0.17 mm$^2$ |

Fig. 20 shows a comparison between the simulated and measured average gains. In general, all the simulated and measured results, are closely matched. Table 1 compares the performance obtained with this prototype and previous works on passive phase shifters.

As can be seen, our work achieved a low insertion loss when compared with others having approximately the same frequency operation, except for [21], but it did not have amplitude control capability. Regarding the RMS phase and gain errors, ours has the lowest values, except for [22], which has a lower RMS phase error; however, this also does not have amplitude control capability.

## V. CONCLUSION

A new passive VMPS was proposed in this work. The cascaded combination of two blocks, the RTBVA and the RTPS, compensate for the low range of phase variation found in RTPSs and simultaneously allow the control of the amplitude. This polar-based configuration results in a simpler and more compact circuit, halving the number of blocks required in a conventional IQ-RTVM. This new architecture was validated by simulations and fabricated on a PCB to operate at a central frequency of 3.6 GHz. The obtained measurements were consistent with the simulation results. By simultaneously combining the characteristics of low insertion loss, low amplitude and phase errors, and amplitude control capability, our work stands out from the remaining state-of-the-art.

## REFERENCES

[1] W. Hong, "Multibeam antenna technologies for 5G wireless communications," *IEEE Trans. Antennas Propag.*, vol. 65, no. 12, pp. 6231–6249, Dec. 2017.

[2] G. M. Rebeiz and L. M. Paulsen, "Advances in SATCOM phased arrays using silicon technologies," in *IEEE MTT-S Int. Microw. Symp. Dig.*, Jun. 2017, pp. 1877–1879.

[3] B. Sadhu, "A 28-GHz 32-element TRX phased-array IC with concurrent dual-polarized operation and orthogonal phase and gain control for 5G communications," *IEEE J. Solid-State Circuits*, vol. 52, no. 12, pp. 3373–3391, Dec. 2017.

[4] T. Hall, B. T. Nukala, C. Stout, N. Brewer, J. Tsay, J. Lopez, R. E. Banister, T. Nguyen, and D. Y. C. Lie, "A phased array non-contact vital signs sensor with automatic beam steering," in *IEEE MTT-S Int. Microw. Symp. Dig.*, May 2015, pp. 1–4.

[5] B. Pillans, S. Eshelman, A. Malczewski, J. Ehmke, and C. Goldsmith, "Ka-band RF MEMS phase shifters," *IEEE Microw. Guided Wave Lett.*, vol. 9, no. 12, pp. 520–522, Dec. 1999.

[6] N. S. Barker and G. M. Rebeiz, "Distributed MEMS true-time delay phase shifters and wide-band switches," *IEEE Trans. Microw. Theory Techn.*, vol. 46, no. 11, pp. 1881–1890, Nov. 1998.

[7] N. Mazor, O. Katz, R. Ben-Yishay, D. Liu, A. V. Garcia, and D. Elad, "SiGe based Ka-band reflection type phase shifter for integrated phased array transceivers," in *IEEE MTT-S Int. Microw. Symp. Dig.*, May 2016, pp. 31–34.

[8] R. Garg and A. S. Natarajan, "A 28-GHz low-power phased-array receiver front-end with 360° RTPS phase shift range," *IEEE Trans. Microw. Theory Techn.*, vol. 65, no. 11, pp. 4703–4714, Nov. 2017.

[9] C.-S. Lin, S.-F. Chang, and W.-C. Hsiao, "A full-360° reflection-type phase shifter with constant insertion loss," *IEEE Microw. Wireless Compon. Lett.*, vol. 18, no. 2, pp. 106–108, Feb. 2008.

[10] T.-W. Li and H. Wang, "A millimeter-wave fully integrated passive reflection-type phase shifter with transformer-based multi-resonance loads for 360° phase shifting," *IEEE Trans. Circuits Syst. I, Reg. Papers*, vol. 65, no. 4, pp. 1406–1419, Apr. 2018.

[11] L. M. Devlin and B. J. Minnis, "A versatile vector modulator design for MMIC," in *IEEE MTT-S Int. Microw. Symp. Dig.*, May 1990, pp. 519–521.

[12] F. Ellinger, U. Mayer, M. Wickert, N. Joram, J. Wagner, R. Eickhoff, I. Santamaria, C. Scheytt, and R. Kraemer, "Integrated adjustable phase shifters," *IEEE Microw. Mag.*, vol. 11, no. 6, pp. 97–108, Oct. 2010.

[13] D. Pepe and D. Zito, "Two mm-wave vector modulator active phase shifters with novel IQ generator in 28 nm FDSOI CMOS," *IEEE J. Solid-State Circuits*, vol. 52, no. 2, pp. 344–356, Feb. 2017.

[14] Z. Peng, L. Ran, and C. Li, "A 24-GHz low-cost continuous beam steering phased array for indoor smart radar," in *Proc. IEEE 58th Int. Midwest Symp. Circuits Syst. (MWSCAS)*, Aug. 2015, pp. 1–4.

[15] A. E. Ashtiani, S.-I. Nam, A. d'Espona, S. Lucyszyn, and I. D. Robertson, "Direct multilevel carrier modulation using millimeter-wave balanced vector modulators," *IEEE Trans. Microw. Theory Techn.*, vol. 46, no. 12, pp. 2611–2619, Dec. 1998.

[16] F. Tabarani and H. Schumacher, "A novel compact balanced reflect-type vector modulator topology," in *Proc. IEEE Bipolar/BiCMOS Circuits Technol. Meeting (BCTM)*, Oct. 2017, pp. 46–49.

[17] U. Mayer, M. Wickert, R. Eickhoff, and F. Ellinger, "2–6-GHz BiCMOS polar-based vector modulator for *S*- and *C*-band diversity receivers," *IEEE Trans. Microw. Theory Techn.*, vol. 60, no. 3, pp. 567–573, Mar. 2012.

[18] E.-T. Sung, S. Wang, and S. Hong, "A 60-GHz polar vector modulator with lookup table-based calibration," *IEEE Microw. Wireless Compon. Lett.*, vol. 31, no. 6, pp. 572–574, Jun. 2021.

[19] Z. Wei, X. Chen, X. Zhu, P.-L. Chi, R. Xu, and T. Yang, "Novel passive vector-sum amplitude-variable phase shifter with integrated reconfigurable filtering function," *IEEE Trans. Microw. Theory Techn.*, vol. 70, no. 7, pp. 3511–3523, Jul. 2022.
[20] C.-H. Chang, J.-Y. Chen, C.-T. Shen, M.-J. Tsai, and T.-S. Tai, "Reflection-type phase shifter integrated with tunable power attenuation mechanism for sub-6 GHz wireless applications," *IEEE Access*, vol. 10, pp. 115532–115540, 2022.
[21] F. Burdin, Z. Iskandar, F. Podevin, and P. Ferrari, "Design of compact reflection-type phase shifters with high figure-of-merit," *IEEE Trans. Microw. Theory Techn.*, vol. 63, no. 6, pp. 1883–1893, Jun. 2015.
[22] J. Xia, M. Farouk, and S. Boumaiza, "Digitally-assisted 27–33 GHz reflection-type phase shifter with enhanced accuracy and low IL-variation," in *Proc. IEEE Radio Freq. Integr. Circuits Symp. (RFIC)*, Jun. 2019, pp. 63–66.
[23] M. Kadam, G. S. Member, and A. Kumar, "A 28 GHz reflective-type transmission-line-based," *IEEE Trans. Circuits Syst. I, Reg. Papers*, vol. 67, no. 12, pp. 4641–4650, Aug. 2020.

**RAUL ARRUELA** (Graduate Student Member, IEEE) was born in Porto, Portugal, in 1982. He received the M.Sc. degree in electronic and telecommunications engineering from the University of Aveiro, Aveiro, Portugal, in 2018, where he is currently pursuing the Ph.D. degree in electrical engineering with the Department of Electronics, Telecommunications and Informatics. He joined the Instituto de Telecomunicações, in September 2018. His research interests include phase-shifters, vector modulators, analog/hybrid beamforming, mmWaves, power amplifiers, RF frontends, radar, 5G, and SATCOM.

**TIAGO VARUM** (Member, IEEE) was born in Estarreja, Portugal, in 1987. He received the M.Sc. degree in electronic and telecommunications engineering and the Ph.D. degree in electrical engineering from the Universidade de Aveiro, Aveiro, Portugal, in 2010 and 2016, respectively. He is currently a Researcher with the Instituto de Telecomunicações, Aveiro, Portugal. His research interests include antenna design, reconfigurable antennas, 3D-printed antennas, non-uniform antenna arrays, beamforming and smart/adaptive antennas for mmWave applications (radar, 5G or SATCOM). He has participated in several projects, has published several papers, in this field, in conference proceedings and journals, and has been a reviewer for several journals and international conferences. He is a member of the IEEE Antennas and Propagation Society.

**JOÃO NUNO MATOS** (Member, IEEE) was born in Oliveira de Azeméis, Portugal, in 1959. He received the bachelor's degree in electronic and telecommunications engineering from the University of Aveiro, Portugal, in 1982, the master's degree in electrical science from the University of Coimbra, Portugal, in 1989, and the Ph.D. degree in electrical engineering from the University of Aveiro, in 1995. He has worked twice in the industry with Portugal Telecom Innovation, Aveiro, Portugal, from 1982 to 1983, and with Ensa Electronic, Madrid, Spain, in 1990. From 1998 to 2000, he was the Head of the Electronics and Telecommunications Department, Aveiro University, where he is currently an Associate Professor and a Senior Researcher at the Instituto de Telecomunicações. He is the author or coauthor of over 100 international conference and journals papers. While the Instituto de Telecomunicações, he participated or led dozens of research's projects in RF/microwave (MW) circuits, system design, and system integration. His current research interests include satellite communications and radars with a special focus on front-end and smart antennas and engineering education.

He is a member of several scientific committees of conferences and journals, as well as professional organizations, and is currently on the Executive Committee of the IEEE Portugal Education Chapter (2019 IEEE Education Society Chapter Achievement Award).